14th International Conference on Structural Safety and Reliability - ICOSSAR'25
1-6 June, 2025 - Los Angeles California, USA
R. Ghanem, E. Johnson, S. Masri and A. Olivier (Eds)

UNCERTAINTY QUANTIFICATION OF THE CONCRETE MODULUS OF ELASTICITY TROUGH DIFFERENT EXPERIMENT TESTS AND SENSORS

Juan Manuel Orozco[1], **Albert R. Ortiz**[2] **Peter Thomson**[3]

[1] Undergraduate Student
Calle 13 # 100-00, Santiago de Cali, Valle del Cauca, Colombiaa
orozco.juan@correounivalle.edu.co

[2] Professor
Calle 13 # 100-00, Santiago de Cali, Valle del Cauca, Colombia
albert.ortiz@correounivalle.edu.co

[3] Professor
Calle 13 # 100-00, Santiago de Cali, Valle del Cauca, Colombia
peter.thomson@correounivalle.edu.co

Key words: Concrete modulus of elasticity, Uncertainty quantification, Mechanical properties, Bayesian inference, likelihood, Posterior Distribution Function (PDF), Digital Image Correlation (DIC).

Abstract. The mechanical properties of construction materials, particularly the Modulus of Elasticity, are fundamental for estimating the structural response and, therefore, a key component in the design and analysis of buildings. Traditional test methods for estimating the Modulus of Elasticity of Concrete involve using ASTM-based specifications based on assumptions and simple compression tests. However, even in single test specimens, methodologies may vary significantly in the number of samples, affecting the likelihood of estimating the Modulus. This research aims to quantify the uncertainty associated with the Modulus of Elasticity of Concrete upon different test setups through Bayesian uncertainty quantification. The study utilizes experimental data obtained from multiple sensors, including Digital Image Correlation (DIC), strain gauges, and Linear Variable Differential Transducers (LVDTs), to provide robust and comprehensive analysis. This research highlights the challenges and biases in characterizing the mechanical behavior of materials commonly used in the construction industry. The findings emphasize the critical role of uncertainty quantification in improving structural safety and reliability, particularly in a context where big data associated with material performance are significantly available. Furthermore, the study discusses the application of ASTM methodologies in a stochastic fashion.

1 INTRODUCTION

In structural engineering, the study of uncertainties and the concept of structural reliability are considered fundamental aspects for the correct evaluation and design of safe and sustainable structures [1]. As the understanding of material properties advances, accurate quantification of the uncertainty inherent in materials becomes essential to ensure that designs are not only functional, but also resilient to unpredictable variations that may arise during their service life.

Several studies have highlighted the importance of accounting for uncertainty in these parameters to enhance structural reliability. For example, Ortiz et al. [2] characterized the uncertainty associated with the standard expressions used to estimate the concrete modulus of elasticity in Colombia, demonstrating that variability in compressive strength and density can significantly skew E estimates; Quimbay Herrera [3] investigated how variations in aggregate properties and curing processes influence the modulus of elasticity of both concrete and mortar, especially under extreme temperature conditions; and Sánchez Oñate et al. [4] showed that using local aggregates from the San Roque mine in Ecuador can produce experimental static modulus values up to 40 % lower than those predicted by ACI-based formulas.

The integration of probabilistic methodologies for uncertainty quantification has opened new possibilities in the structural reliability analysis and material property estimation fields. In particular, the use of Bayesian probabilistic models has been shown to be a powerful tool for fitting experimental data and estimating parameters such as the modulus of elasticity in a probabilistic fashion. These models allow incorporating prior knowledge and adjusting the probability distributions of the parameters as more experimental data are collected, which improves the predictive capability of the models.

The present work focuses on the quantification of the uncertainty in the calculation of the modulus of elasticity of concrete, using Bayesian probabilistic models to process the data obtained experimentally from a concrete cylinder tested in compression. This cylinder was instrumented with strain gauges, LVDT and Digital Image Correlation (DIC). This study aims to advance the understanding of the variability of concrete and provide a more accurate and reliable methodology for the calculation of the modulus of elasticity, which could be applied to future structural design and reliability analysis projects.

The remainder of this paper is organized as follows. Section 2 introduces the theoretical framework for static modulus estimation and Bayesian adjustment, including the ASTM-C469 and vector models. Section 3 details the experimental methodology, describing the concrete cylinder test and sensor instrumentation. Section 4 presents the uncertainty quantification results, with posterior distributions of the modulus of elasticity. Section 5 analyzes and interprets these findings in the context of structural reliability. Finally, Section 6 summarizes the conclusions and outlines directions for future work.

2 THEORETICAL FRAMEWORK

2.1 ACI-C469 Static Modulus Estimation

According to ACI 318-14, the static modulus of elasticity of normal-weight concrete, E_c, can be estimated from the compressive strength f'_c by:

$$E_c = 4700\sqrt{f'_c} \quad (\text{MPa}), \tag{1}$$

where f'_c is in MPa. In the ASTM C469 "two-point" method, E is defined by two points on the stress–strain curve:

$$E = \frac{S_2 - S_1}{\epsilon_2 - \epsilon_1}, \tag{2}$$

with

- S_1: stress at fixed strain $\epsilon_1 = 0.00005$,
- $S_2 = 0.4\, f'_c$: stress at 40% of the peak load,
- ϵ_2: corresponding strain at S_2.

Sensor specification. ASTM C469 prescribes measurement of ϵ_1 and ϵ_2 using a single strain gauge and two LVDTs only. In this work, we extend the standard protocol by incorporating Digital Image Correlation (DIC), which—rather than yielding a single strain value per load level—produces a full-field strain matrix over the defined area of interest. This richer spatial information enhances the robustness and noise resistance of the modulus estimation compared to the traditional two-sensor setup.

2.2 Bayesian Adjustment Theory

Bayesian inference provides a coherent framework to update model parameters θ (here, modulus E and noise σ) given data D. Bayes' theorem states:

$$p(\theta \mid D) \;=\; \frac{p(D \mid \theta)\, p(\theta)}{p(D)}, \tag{3}$$

where

- $p(\theta)$ is the **prior** distribution encoding existing knowledge,
- $p(D \mid \theta)$ is the **likelihood**, describing how probable the data are given θ,
- $p(\theta \mid D)$ is the **posterior** distribution, our updated belief after observing D,
- $p(D)$ is the evidence (normalizing constant).

2.3 Definition of Bayesian Models

Two Bayesian models were constructed to infer E from experimental stress–strain data:

2.3.1 ASTM-C469 Model (Two-Point)

- Two key points (ϵ_1, S_1) and (ϵ_2, S_2) were selected as in equation (2).
- Each pair was cast into vectors (for DIC, each value was repeated n times) and concatenated into arrays.
- These arrays were used to define a Bayesian model in PyMC—a Python library for probabilistic programming that allows one to specify priors, likelihoods, and perform Markov chain Monte Carlo (MCMC) sampling—so as to infer the posterior distribution of the modulus E.

2.3.2 Vector Model (All Points of the Linear Range)

- *All* data points that lie within the linear elastic region of the stress–strain curve were used.
- This approach harnesses more observations to tighten posterior uncertainty, at the cost of increased computational effort.

In both cases, MCMC sampling in PyMC yields posterior distributions for E and σ, from which credible intervals and posterior predictive checks are derived [1, 5].

3 METHODOLOGY

In the present work, as mentioned above, a concrete cylinder was tested under compression by applying a constant axial load over the entire surface of the cylinder.

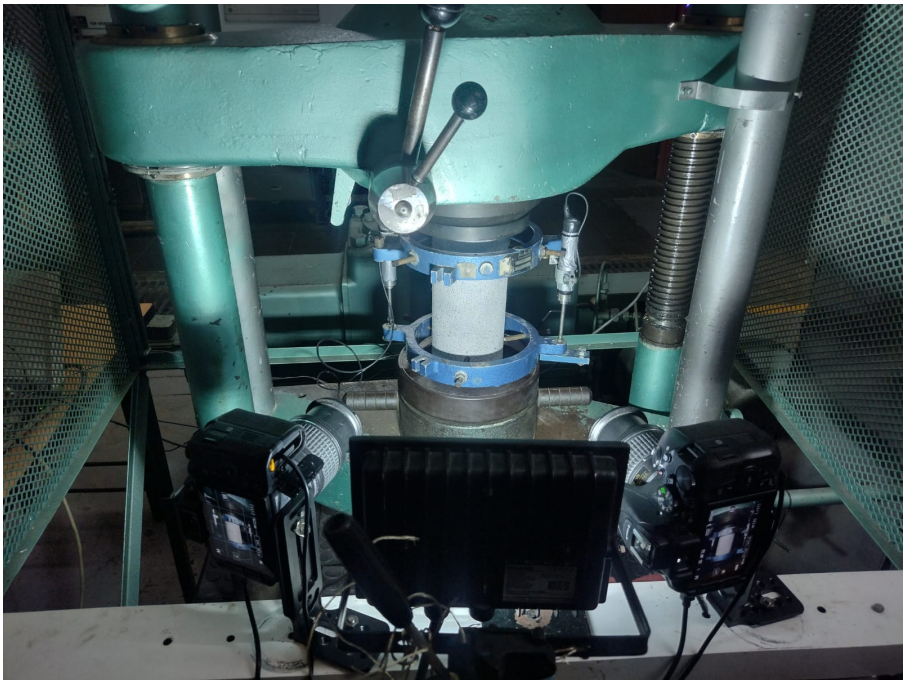

Figure 1: Cylindrical test setup

The specimen, of cylindrical section, had a height of 8 inches and a diameter of 4 inches. It was made with the same mix used in a previous project on uncertainty quantification in reinforced concrete

beam models, carried out at the School of Civil Engineering and Geomatics of the Universidad del Valle. The sample was properly vibrated, cured and molded as homogeneously as possible, in order to minimize the uncertainty derived from human manipulation.

Once demolded and cured, the specimen was instrumented. For this purpose, a strain gauge was installed on the opposite side. A speckle pattern was applied with spray for the area of interest of the DIC. It is essential to properly distribute the measurement points of the different sensors on the cylinder to avoid interference in data capture. In addition, two LVDTs were installed as shown in Figure 1, one on each side of the cylinder, for the purpose of obtaining accurate readings in case the cylinder rotated due to load adjustment on the universal machine. This is one of the recommendations stipulated by ASTM-C469 standard for taking deformation data on concrete cylinders. Simultaneously, a block diagram was programmed in *Simulink* to acquire the data in real time from the sensors to the acquisition system connected to the computer.

The strain gauge, with a length of 3.54 inches, was placed in the longitudinal direction of the cylinder. The speckle pattern was applied in an area spanning 120 degrees along the entire height. Two Nikon D5600 cameras were used, positioned so that they formed a 20-degree angle to each other, at a distance of 12 inches from the cylinder to the lens of each. The cameras' resolution of 6000 x 4000 pixels ensured a high level of detail in capturing the deformations, allowing points between 3 and 5 pixels in size to be identified. A high-power LED panel located halfway between the two cameras was also used, oriented directly to the area of interest for the DIC. A block was programmed in Simulink that simultaneously triggered both cameras every 5 seconds.

4 RESULTS

An area of interest was defined on the specimen and imaged simultaneously by both DIC cameras to ensure accurate point-to-point correlation and minimize measurement noise. The following figure illustrates the unit strain distribution computed over that region.

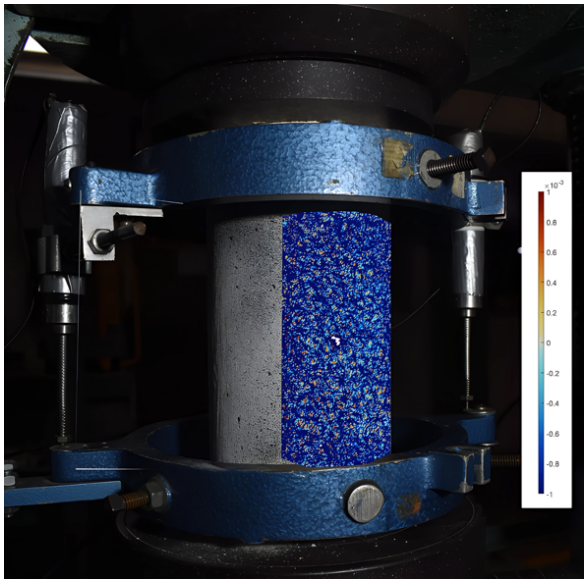

Figure 2: Unit strain distribution on the selected area of interest,

Once the cylinder failed, the deformation results obtained by the gage, LVDT and DIC sensors were recorded. In addition, the trigger signal from both cameras was saved, which allowed synchronizing the instant at which the photographs were taken with respect to the applied load, which was also recorded. With these data, the stress-strain curves corresponding to each method were obtained.

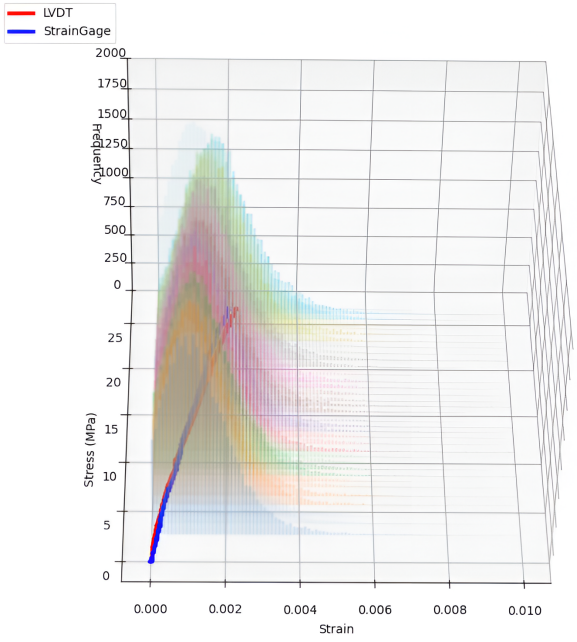

Figure 3: Cylinder stress–strain curves.

As shown in Figure 3, the stress-strain curves obtained from the gauge (in red) and the average of the LVDT strains (in blue) are very similar, which allows us to take them as reference curves for the DIC distributions that usually have a little more problems due to noise issues. On the other hand, the DIC data, unlike the other two sensors that generate a single strain data for each stress state, provided approximately 50,000 data for each photo (every 5 seconds).

Since each DIC distribution generated vectors of 50,000 data, the frequency distribution of the data for each image was plotted to visualize the deformation behavior. Figure 4 shows the frequency distribution corresponding to the first deformed photo (or second global photo, since all the deformed images are compared with the reference photo, i.e., photo 1). As can be seen, the distribution of unit deformations presents, in general, positive values; however, some noise is always observed due to phenomena such as tangential distortion and changes in illumination during the test. Although a calibration of the chambers was performed to correct these errors, the noise remains and must be considered in the analysis.

It is mandatory to use only data from the linear phase of the stress–strain curve and first visualize

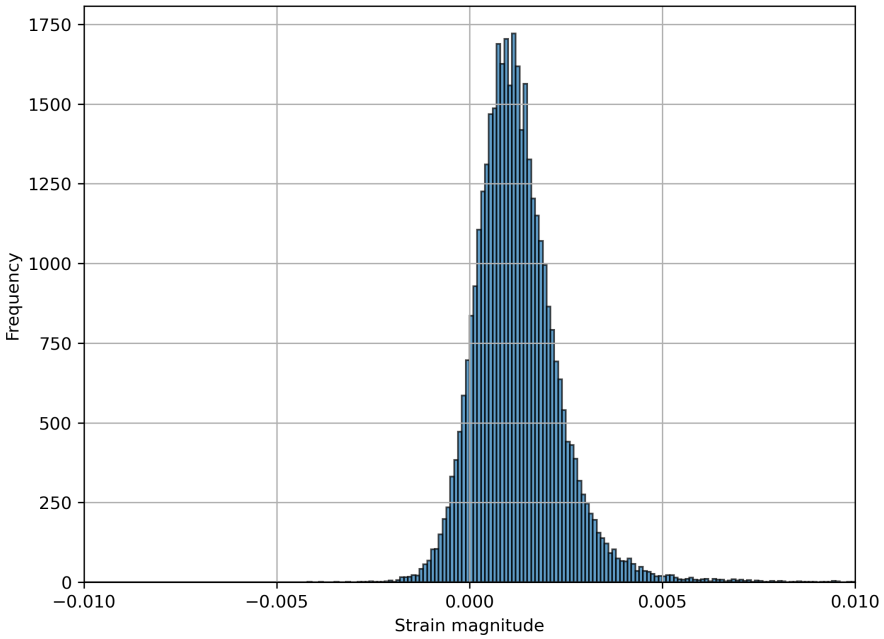

Figure 4: Frequency distribution for the first deformed photo

their behavior to identify truly linear points before applying the Bayesian adjustment. For the fitting process, it was necessary to define two different Bayesian fitting functions as mentioned in the theoretical framework. One important note regarding **Figure 2** is that, by convention, compressive strains are initially recorded as negative values; these were converted to positive values during the post-processing stage.

4.1 Bayesian fitting function for gages and LVDTs

As for the definition of the Bayesian approach, the fitting process was developed using the library known as PyMC available in the Python language. The process flow for the definition of the Bayesian fitting function for Gauges and LVDT is shown below. A normal distribution of mean 18000 MPa and a standard deviation of 10000 MPa was defined for the modulus of elasticity.

Algorithm 1 Bayesian adjustment for strain gauges and LVDTs

Input: Strain vector $\epsilon = \{\epsilon_1, \epsilon_2, \ldots, \epsilon_n\}$, stress vector $f = \{f_1, f_2, \ldots, f_n\}$, and prior modulus E_{prior}.
Procedure: Linear model
  Priors:
    $E \sim \text{Normal}\big(\mu = E_{\text{prior}},\, \sigma = 10000\big)$
    $\sigma \sim \text{Uniform}(0,\, 20)$
  Model:
    $f_{\text{estimated}} = E \cdot \epsilon$
  Likelihood:
    $\text{Likelihood}_{\text{linear}} = \text{Normal}\big(\mu = f_{\text{estimated}},\, \sigma = \sigma,\, \text{observed} = f\big)$
  Initial values:
    $\text{start} = (E = E_{\text{prior}},\, \sigma = 10)$
  Sampling:
    $\text{trace} = \text{sample}(1000,\, \text{tune} = 500,\, \text{start} = \text{start})$
End procedure
Output: trace

4.2 Bayesian fitting function for DIC

It was necessary to define a Bayesian fitting function different from that of gauge and LVDT due to the distribution of their data, since as mentioned above, there are about 50,000 data for each stress state of which some are negative values of deformation, in addition to the noise present in the data. This is why it was necessary to make some small modifications to the distribution types for the priors and likelihood using more rigorous distributions in order to obtain a good convergence in the MAP values. A StudentT type likelihood distribution was used, which allows giving more weight to the most repeated strain values, leaving aside those outliers present in the strain distributions. The use of this distribution has been recommended in the official PyMC website for robust linear regression models or in articles such as Kruschke's article [5].

Similarly, it should be noted that for the input data of the Bayesian model it was necessary to make an additional cleaning of the data, since as shown in Figure 3, there are both negative data and data influenced by the noise of the software processing for all photos from the first deformed photo. Initially a debugging of the deformation data obtained from the triangle mesh of the *Triangular Cosserat Point* method was performed, which is a method implemented in the DuoDIC software code [6] to perform a meshing of the area of interest, see more in the article published by Dana Solav where it is explained in detail how this method works [7]. Once the negative strain values that greatly affect the Bayesian fit were removed and a noise constant of 0.0008 was subtracted from the unit strain values, the following Bayesian fit function was proposed for the DIC data. A prior for the modulus of elasticity of 18000 MPa was also defined.

Algorithm 2 Bayesian adjustment for DIC data

Input: Data vectors: strain $\epsilon = \{\epsilon_1, \epsilon_2, \ldots, \epsilon_n\}$, stress $f = \{f_1, f_2, \ldots, f_n\}$, and prior modulus E_{prior}.
Procedure: Linear model
  Priors:
    $E \sim \text{TruncatedNormal}\big(\mu = E_{\text{prior}},\ \sigma = 2000,\ \text{lower} = 5000,\ \text{upper} = 30000\big)$
    $\sigma \sim \text{HalfNormal}(\sigma = 40)$
  Model:
    $f_{\text{estimated}} = E \cdot \epsilon$
  Likelihood:
    $\text{Likelihood}_{\text{linear}} = \text{StudentT}\big(\nu = 4,\ \mu = f_{\text{estimated}},\ \sigma = \sigma,\ \text{observed} = f\big)$
  Initial values:
    $\text{start} = (E = E_{\text{prior}},\ \sigma = 10)$
  Sampling:
    $\text{trace} = \text{sample}(1000,\ \text{tune} = 500,\ \text{start} = \text{start})$
End procedure
Output: trace

4.2.1 Results of ASTM-C469 model posterior distributions

Our Bayesian fitting functions for both gauges, LVDT and DIC allow us to obtain as output variables the posterior distributions of: Modulus of elasticity, sigma of the model and its posterior predictive check (PPC). However, for space reasons in this paper we will only show the results of modulus of elasticity. The results are shown below:

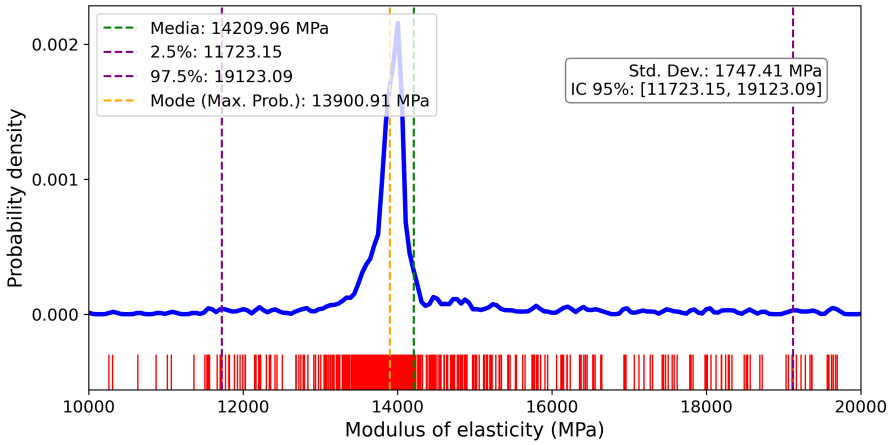

Figure 5: Posterior distribution of modulus of elasticity E for LVDT model ASTM-C469

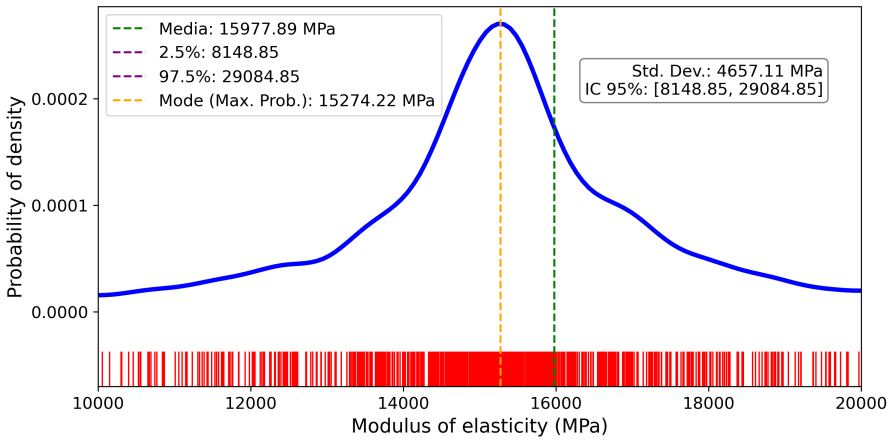

Figure 6: Posterior distribution of the modulus of elasticity E for ASTM-C469 model gauge.

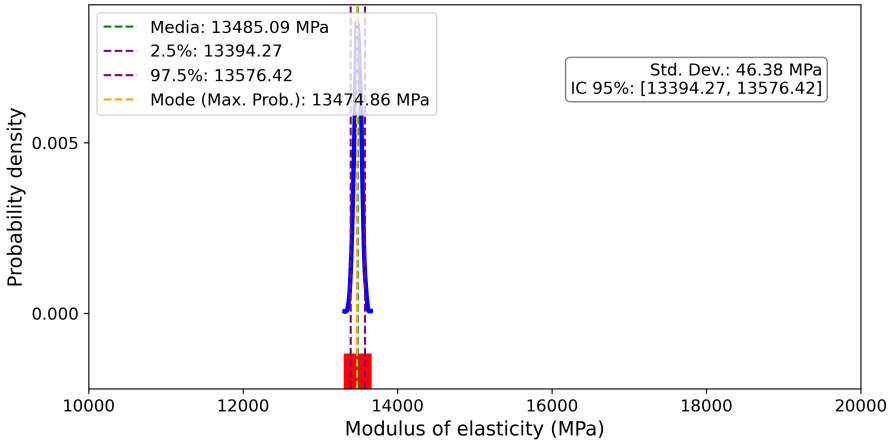

Figure 7: Posterior distribution of modulus of elasticity E for DIC model ASTM-C469

4.2.2 Results of posterior distributions vector type model

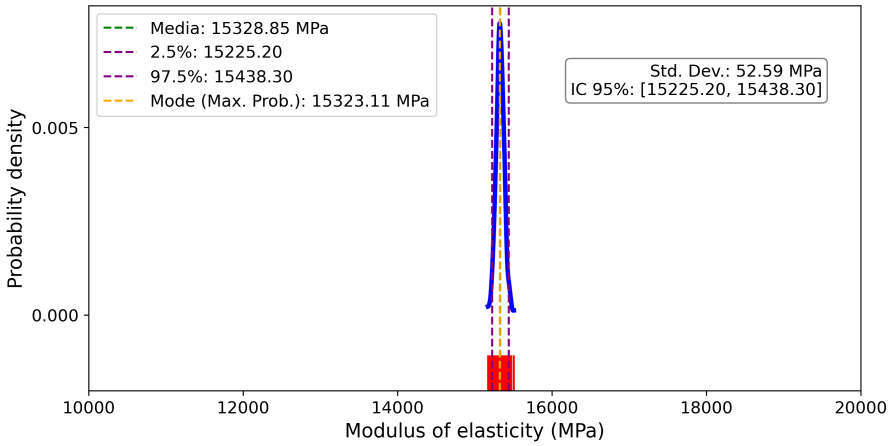

Figure 8: Posterior distribution of modulus of elasticity E for LVDT vector model

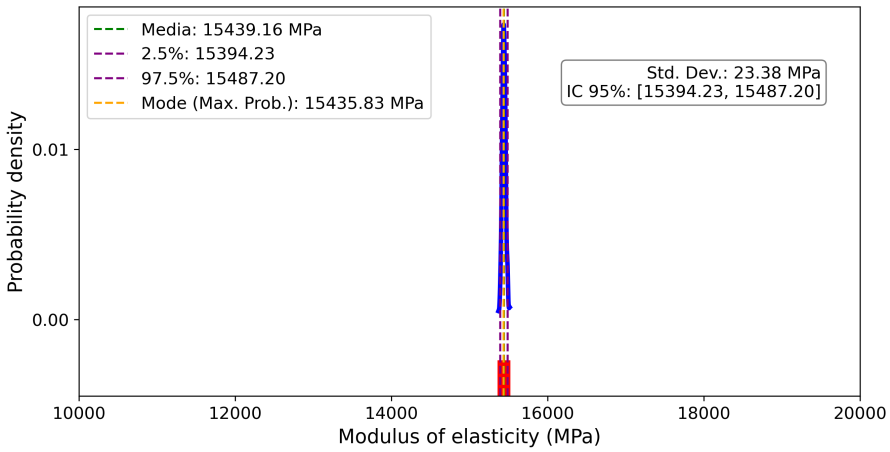

Figure 9: Posterior distribution of modulus of elasticity E for gauge vector model

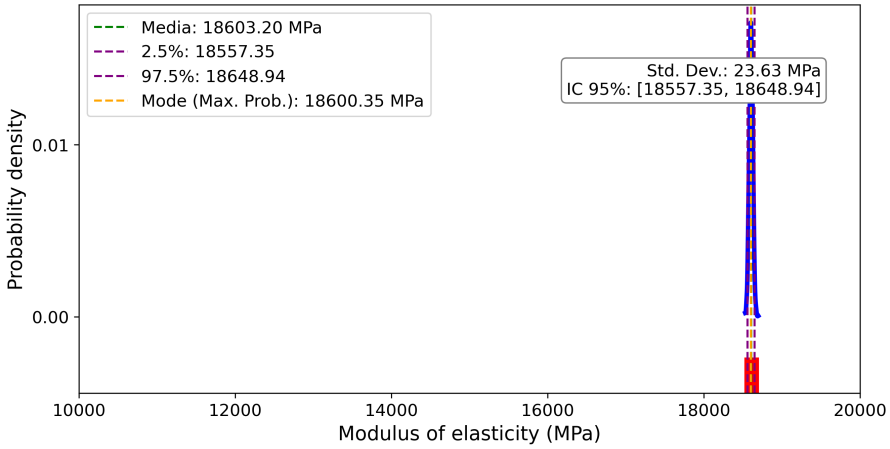

Figure 10: Posterior distribution of modulus of elasticity E for DIC vector model

5 RESULTS ANALYSIS

Under the ASTM-C469 model, the posterior distributions of E exhibit marked differences between sensor types. For strain gauges and LVDTs—each based on only two data points—the coefficient of variation (COV = σ/μ) spans roughly 7 % to 35 %, reflecting very high relative uncertainty. By contrast, the DIC two-point approach, despite also using two stress levels, yields a COV below 5 %, demonstrating that the large number of strain measurements per load state greatly enhances the reliability of the estimated modulus once noise is filtered.

As for the vector type model, a clear reduction of the standard deviation is evidenced for all the sensors. The gauge and the LVDT remain around a modulus of elasticity of 15000 MPa where an increase in its modulus value E was evidenced. In the subsequent distribution of the DIC, a significant increase is observed between models, going from 13000 MPa approximately to 18000 MPa, also reducing its standard deviation.

6 CONCLUSIONS

Notably, DIC—thanks to its extremely high spatial and temporal resolution—provides very precise estimates (small posterior bias), although it can under-estimate the modulus under the "two-point" approach compared to gauge and LVDT methods. The latter, while exhibiting greater dispersion (higher uncertainty), yield consistent mean values that bolster our confidence in the true magnitude of E.

For the vector model, by incorporating all data corresponding to the linear phase of the stress–strain curve, the vector model substantially increased the information available for Bayesian fitting. This increase in data reduced the standard deviation of the posterior distribution by approximately 30–50 % for the three measurement systems, confirming that more linear observations improve the accuracy of E. In particular, the DIC under the vector model showed an increase in the mean value of E (from 13,000 MPa to 18,000 MPa) and a notable reduction in its bias, demonstrating that the use of multiple points corrects the underestimation of the ASTM approach.

7 ACKNOWLEDGMENTS

Special acknowledgements to the support of the 3D Printing Project at the School of Civil Engineering and Geomatics, Universidad del Valle, for providing the equipment and expertise that were essential to this research.

REFERENCES

[1] Beck, J. L.; Au, S. K. (2002). Bayesian updating of structural models and reliability using Markov chain Monte Carlo simulation. *Journal of Engineering Mechanics*, 128(4), 380–391. DOI:10.1061/(ASCE)0733-9399(2002)128:4(380).

[2] Ortiz, A. R.; Carrillo, J. (2025). Uncertainty of Models for Modulus of Elasticity of Concrete in Colombian Code. *ACI Materials Journal*, **122**(2), 3–13. DOI:10.14359/51745620.

[3] Quimbay Herrera, R. (2020). *Estimación del módulo de elasticidad del concreto y del mortero mediante TCTM*. Universidad Nacional de Colombia, Bogotá, Colombia.

[4] Sánchez Oñate, D. M.; Chiliquinga Cando, J. P.; Flores Montalvo, E. P.; Orosco Tacuri, M. K. (2020). Módulo estático de elasticidad del hormigón fabricado con agregados de la mina de San Roque, Imbabura, Ecuador. *Revista Politécnica*, **46**(1), 29–38. DOI:10.33333/rp.vol46n1.03.

[5] Kruschke, J. K. (2014). *Doing Bayesian Data Analysis: A Tutorial with R, JAGS, and Stan*. Academic Press.

[6] Solav, D., & Silverstein, A. (2022). *DuoDIC: 3D Digital Image Correlation in MATLAB*. Journal of Open Source Software, 7(74), 4279. https://doi.org/10.21105/joss.04279

[7] Solav, D., Rubin, M. B., Cereatti, A., Camomilla, V., & Wolf, A. (2016). *Bone Pose Estimation in the Presence of Soft Tissue Artifact Using Triangular Cosserat Point Elements*. Annals of Biomedical Engineering, 44(4), 1181–1190. https://doi.org/10.1007/s10439-015-1384-6